NASA Contractor Report 187542
ICASE Report No. 91-32

ICASE

THE P^1— RKDG METHOD FOR TWO-DIMENSIONAL EULER EQUATIONS OF GAS DYNAMICS

Bernardo Cockburn
Chi-Wang Shu

Contract No. NAS1-18605
March 1991

Institute for Computer Applications in Science and Engineering
NASA Langley Research Center
Hampton, Virginia 23665-5225

Operated by the Universities Space Research Association

National Aeronautics and
Space Administration

Langley Research Center
Hampton, Virginia 23665-5225

THE P^1 – *RKDG* METHOD FOR TWO-DIMENSIONAL EULER EQUATIONS OF GAS DYNAMICS

Bernardo Cockburn[1]
School of Mathematics
University of Minnesota
Minneapolis, MN 55455

and

Chi-Wang Shu[2]
Division of Applied Mathematics
Brown University
Providence, Rhode Island 02912

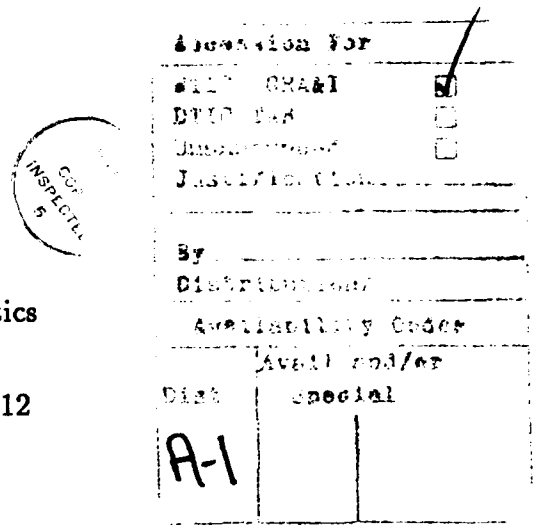

ABSTRACT

We continue our earlier work on a class on nonlinearly stable Runge-Kutta local projection discontinuous Galerkin (RKDG) finite element methods for conservation laws. Two-dimensional Euler equations for gas dynamics are solved using P^1 elements. We discuss the generalization of the local projection, which for scalar nonlinear conservation laws was designed to satisfy a local maximum principle, to systems of conservation laws such as the Euler equations of gas dynamics using local characteristic decompositions. Numerical examples include the standard regular shock reflection problem, the forward facing step problem and the double Mach reflection problem. These preliminary numerical examples are chosen to show the capacity of our approach to obtain nonlinearly stable results comparable with the modern nonoscillatory finite difference methods. Generalizations to P^k elements with $k > 1$ and the use of adaptive triangulations to minimize local errors constitute ongoing research.

[1]Partially supported by the Army High Performance Computing Research Center, FMC Technology Center Building, 1300 South Second Street, Minneapolis, MN 55454 and by a Grant of the Minnesota Supercomputer Institute, 1200 Washington Avenue South, Minneapolis, MN 55455.

[2]Research was supported by the National Aeronautics and Space Administration under NASA Contract No. NAS1-18605 while the author was in residence at the Institute for Computer Applications in Science and Engineering (ICASE), NASA Langley Research Center, Hampton, VA 23665. Support was also provided by NSF Grant DMS-8810150, NASA Langley Grant NAG-1-1145, and AFOSR Grant 90-0093.

1. Introduction. In this paper we continue our earlier work [C1], [C2], [C3], [C4], of constructing and analyzing a class of discontinuous Galerkin finite element method for solving conservation laws

$$\mathbf{u}_t + \sum_{i=1}^{d} (\mathbf{f}_i(\mathbf{u}))_{x_i} = 0, \tag{1.1}$$

equipped with suitable initial or initial–boundary conditions. We concentrate on two-dimensional Euler equations of gas dynamics, i.e., in (1.1) with $d = 2$, $\mathbf{u} = (\rho, \rho q_x, \rho q_y, E)^t$, $\mathbf{f}_1(\mathbf{u}) = q_x \mathbf{u} + (0, p, 0, q_x p)^t$, $\mathbf{f}_2(\mathbf{u}) = q_y \mathbf{u} + (0, 0, p, q_y p)^t$, where q_x, q_y are the velocity components in the x and y directions, ρ is the density, E is the total energy, $p = (\gamma - 1)(E - \frac{1}{2}\rho(q_x^2 + q_y^2))$ is the pressure, and $\gamma = 1.4$ for the air.

One distinctive feature of our approach is a local projection limiting which borrows the successful non-oscillatory finite difference methodology, guarantees total variation boundedness (TVB) for one-dimensional nonlinear scalar equations and linear systems, and yields a local maximum principle for multi-dimensional scalar equations. Another feature of our approach is the use of high-order total variation diminishing (TVD) Runge-Kutta type time discretizations [S1] which renders the scheme explicit (and hence fully parallelizable) and computationally efficient. The general framework was given in [C2] for the nonlinear one-dimensional scalar case. The TVB property and convergence were proven for general P^k elements (which give rise to uniformly $(k+1)$-th order accurate schemes). Numerical results for $k = 1$ and $k = 2$ (second and third order) were shown which gave sharp, monotone shock transitions and uniform high-order accuracy in the smooth part of the solutions. In [C3], we applied the method to the one-dimensional Euler equations of gas dynamics by designing the local projection in the local characteristic fields. The resulting scheme was proven TVB for linear systems with both initial and initial-boundary conditions. Numerical results included both standard shock tube problems and a problem involving the interactions between a Mach 3 shock and a density wave – a prototype for shock-turbulence interactions. In all cases, we obtained results comparable to those obtained by recent nonoscillatory finite difference methods (e.g., [W], [S2]). The crucial generalization to multi-space dimensions was carried out in [C4], where we introduced a local projection limiting which does not have a direct counter-part in the current finite difference schemes, guarantees a local maximum principle for a class of very general triangulation (we called them B-triangulations), and maintains uniform high-order accuracy in the smooth part of the solution. Numerical results showed the potential of the scheme in easy handling general triangulations and boundary conditions.

The organization of this paper is as follows. In §2 we briefly describe the formulation of the scheme. Special attention is paid to the monotone fluxes (approximate Riemann solvers) across the edges of the triangles and to the local projections associated with them, since they are distinct from the scalar case considered in [C4]. In §3 we present numerical results of our P^1-RKDG scheme on the the shock reflection problem, the forward facing

step problem, and the double Mach reflection problem. We end with some concluding remarks in §4.

2. The formulation of the scheme. Suppose we are solving the equation (1.1) ($d = 2$) on a polygonal domain Ω. Let $\mathcal{T}_h = \{K\}$ be a B-triangulation of Ω (see [C4] for the definition), and set $V_h = \{p \in \mathrm{L}^\infty(\Omega) : p|_K \in \mathrm{P}^k(K)\ \forall K \in \mathcal{T}_h\}$ where $\mathrm{P}^k(K)$ is the space of polynomials of total degree less than or equal to k on K. In this paper we only consider $k = 1$, which yields second-order accurate schemes. Notice that the functions in V_h can be discontinuous across the edges of the triangles in $\mathcal{T}_h$. For scalar equations, the discontinuous Galerkin method consists in finding $u_h : [0,T] \mapsto V_h$ satisfying

$$\begin{aligned} \frac{d}{dt}\int_K u_h(t,x)\,v_h(x)\,dx + \sum_{e\in\partial K}\int_e \mathbf{f}(u_h(t,x))\cdot\mathbf{n}_{e,K}\,v_h(x)\,d\Gamma \\ - \int_K \mathbf{f}(u_h(t,x))\cdot\mathbf{grad}\,v_h(x)\,dx = 0, \quad \forall v_h \in V_h, \end{aligned} \tag{2.1}$$

where $\mathbf{n}_{e,K}$ is the outward unit normal to the edge e and $\mathbf{f} = (f_1, f_2)$. This is obtained by multiplying (1.1) with a test function $v_h \in V_h$, integrating over a triangle $K \in \mathcal{T}_h$, integrating formally by parts, and replacing u by its approximation u_h. Since u_h can be discontinuous across an edge e, we replace $\mathbf{f}(u_h(t,x))\cdot\mathbf{n}_{e,K}$ by a monotone flux

$$h_{e,K}(u_h(x^{int(K)}), u_h(x^{ext(K)})), \tag{2.2}$$

which is consistent: $h_{e,K}(u,u) = \mathbf{f}(u)\cdot\mathbf{n}_{e,K}$; monotone: $h_{e,K}(u,v)$ is nondecreasing in u and nonincreasing in v; Lipschitz continuous; and legitimate as a flux:

$$h_{e,K}(u_h(x^{int(K)}), u_h(x^{ext(K)})) = -h_{e,K'}(u_h(x^{int(K')}), u_h(x^{ext(K')})) \text{ for } K' \cap K = e.$$

The line integrals in (2.1) are replaced by the two-point Gauss quadrature rule, and the surface integrals replaced by the mid-point quadrature rule. The resulting O.D.E. is then discretized by the second-order accurate TVD Runge-Kutta method in [S1] and coupled with a local projection applied at the end of each inner step. This local projection is crucial for keeping the nonlinear stability (a local maximum principle) of the scheme; it is described in detail in [C4].

For systems of equations, (2.1) is satisfied by each component of $\mathbf{u}_h$. The monotone flux (2.2), however, is replaced by an approximate Riemann solver: the relevant quantities $\mathbf{f}(u_h(x^{int(K)},t)\cdot\mathbf{n}_{e.K}$ and $\mathbf{f}(u_h(x^{ext(K)},t)\cdot\mathbf{n}_{e,K}$ are left-multiplied by the left eigenvectors of some average Jacobian across e (we use the Roe average [Roe] associated with $\bar{\mathbf{u}}_K$ and $\bar{\mathbf{u}}_{K'}$, the cell averages of $\mathbf{u}$ in K and K' whose common edge is e, in the normal direction to e), the scalar monotone flux (2.2) (we use the local Lax-Friedrichs flux [C2]) is then applied in each of the resulting local characteristic fields, and the results are projected back

by using the right eigenvectors of the same Jacobian. This is essentially a one-dimensional characteristics procedure across the edge e. Details about it can be found in [C3].

Next we describe the local projection. For the scalar case, a local maximum principle can be proven if we compute local approximate gradients using $\bar{\mathbf{u}}_K$ and $\bar{\mathbf{u}}_{K'}$, where K and K' are the immediate and some further away neighbors of K, and use them to limit the deviations of $\mathbf{u}_h$ evaluated at Gaussian points from the mean $\bar{\mathbf{u}}_K$. The limiting is performed in such a way as not to destroy the formal accuracy in smooth regions. The details and proofs can be found in [C4]. For systems of equations, the limiting should be performed in the local characteristic fields. We adopt the simplified version of the local projection which involves only the midpoints of the edges of K instead of all the Gaussian points (as in [C4]) and limits the deviation by considering only the approximate gradient obtained by using $\bar{\mathbf{u}}_K$, $\bar{\mathbf{u}}_{K'_1}$ and $\bar{\mathbf{u}}_{K'_2}$, where K'_1 and K'_2 are the two 'forward' facing triangles adjacent to K; notice that the vector $\mathbf{M} - \mathbf{B}_K$, where $\mathbf{B}_K$ is the barycenter of the triangle K, is a positive combination of the vectors $\mathbf{B}_{K'_1} - \mathbf{B}_K$ and $\mathbf{B}_{K'_2} - \mathbf{B}_K$, see Fig. 1. (In [C4] we used a projection that uses an additional approximate gradient obtained with backward facing elements K'_1 and K'_2. Our numerical experience shows that such a projection is not needed in this framework.) The relaxation factor b, which is the ratio allowed of the deviation of $\mathbf{u}_h$ to $\bar{\mathbf{u}}_K$ over that computed by the approximate gradient, is chosen to be 1.5 ($b > 1$ guarantees second-order accuracy in smooth monotone regions). This simplified projection reduces the computational cost and seems to work well numerically. We again use the Roe average associated with $\bar{\mathbf{u}}_K$ and $\bar{\mathbf{u}}_{K'_1}$, where $K \cap K'_1 = e$, along the normal of e, to perform the characteristic decomposition for the projection limiting at the midpoint of e; see Fig. 1. The projection limiting is done at each midpoint independently form the projections at the other midpoints. Then, a simple readjustment is performed to enforce the conservativity of the method. This renders the projection limiting simple and efficient. In all our computations we took $M = 50$; see [C4].

3. The numerical examples. We use three standard test problems: the regular shock reflection, flow past a forward facing step, and the double Mach reflection problem, to display the behavior of our P^1–RKDG scheme. We run our code on triangulations that are obtained, essentially, by taking the usual finite difference grid and dividing its rectangles into two triangles. (In principle, this should produce a bigger numerical diffusion and a stronger mesh distorsion; on the other hand, these undesirable effects could be counterbalanced by the inherent increase of degrees of freedom. Indeed, this seems to be the case.) The objective is to verify that our scheme gives results comparable to the results given by the recent nonoscillatory finite difference schemes for these standard test problems. Except for the second run in Example 1, we deliberately do not use the alignments of triangles with shock structures in order to carry out a fair comparison with finite difference schemes. For problems involving complicated geometries and/or boundary conditions. the advantages of our finite element schemes over finite difference methods would be more significant. Also, for problems involving both shocks and complicated flow

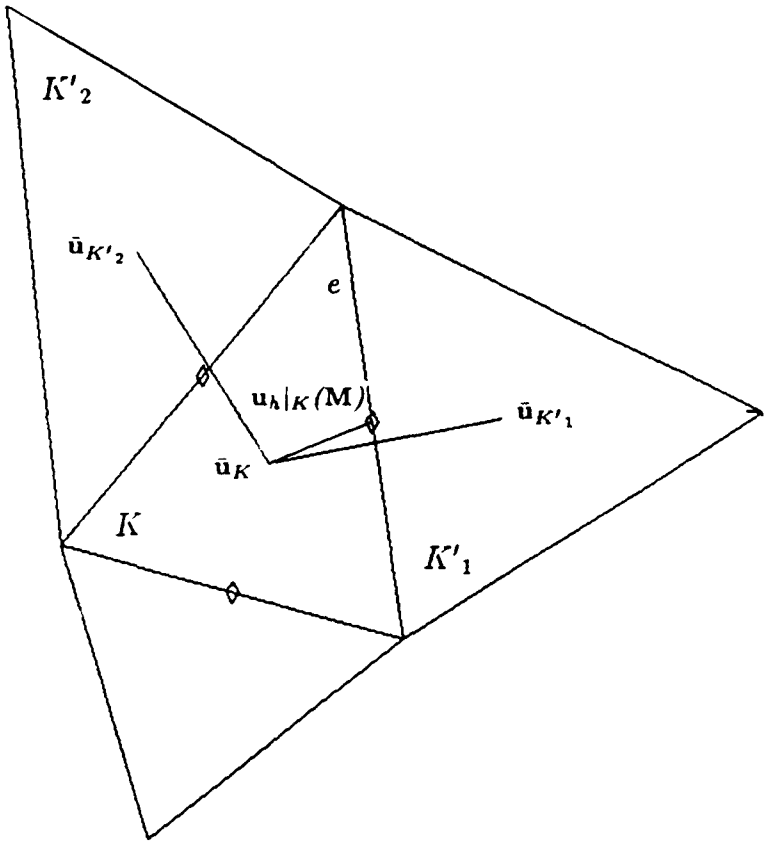

FIG. 1. *Projecting* $u_h|_K(M)$ *at the midpoint* M. *The deviation* $u_h|_K(M)$-$\bar{u}_K$ *is compared with b times the deviation at* M *obtained by the approximate gradient formed with* $\bar{u}_K$, $\bar{u}_{K'_1}$, *and* $\bar{u}_{K'_2}$.

structures, P^k–RKDG schemes would show their advantage in high resolutions. Research along these directions is currently being carried out.

In all our computations we have used the CFL-condition $\Delta t \sup \lambda_K |e|/|K| \leq 0.3$, where λ_K is the modulus of the velocity plus the sound speed evaluated at the barycenter of the traingle K. We use the CRAY2 at the Minnesota Supercomputer Center to carry out our computations. The code is carefully written so that most of the major loops are fully vectorized. Due to the local structure of the algorithm, a parallel version of the CRAY2 code could be written; we plan to do this in the future. Our graphics has been done with the finite element package MODULEF. We have used 30 isovalues in all our contour figures.

Example 1: Regular shock reflection. This well-known example involves an oblique shock reflecting from the lower boundary of a rectangular domain. The computational domain is $0 \leq x \leq 4.12829, 0 \leq y \leq 1$. The initial condition is $\rho = 1, q_x = 2.9, q_y = 0, p = 1/1.4$ throughout the computational domain. The boundary conditions applied are: inflow boundary condition at $x = 0$ (prescribe all components of u_h with

values same as the initial condition); outflow boundary condition at $x = 4.12829$ (all components are freely flowing out); enforcing the post-shock condition at the upper boundary $y = 1(\rho = 1.7, q_x = 2.61932, q_y = -.506339, p = 1.52824)$; and enforcing a reflection boundary condition at the lower boundary $y = 0$ (if an edge e of a triangle is at the lower boundary $y = 0$, then the boundary value of u_h at $(x, y = 0)$ is chosen to be the same as $\mathbf{u}_h$ from $y \mapsto 0^+$ for ρ, q_x, and p but opposite in sign for q_y. The exact solution to this problem is an incoming shock of 29 degrees with the lower boundary and a reflected shock of 23.28 degrees. The exact solution past the second shock should be $\rho = 2.68732$, $q_x = 2.40148$, $q_y = 0$ and $p = 2.93413$.

In Fig. 2b we show the pressure contour computed with a refinement of the triangulation in Fig. 2a corresponding to the uniform Cartesian grid '$\Delta x = \Delta y = 1/40$.' Notice how the incident shock is approximated much better that the reflected one. This is due to the fact that the triangles are partially aligned with the incident shock and cut the reflected shock, increasing in this case the numerical diffusion; see Fig. 2b. In order to see how dramatically the result can improve when triangles are perfectly aligned with the shocks, we show in Fig. 2d the pressure contour computed with the triangulation in Fig. 2c. In this case, the L^1-error (with only three triangles) is only ten times bigger than the L^1-error produced by the approximation displayed on Fig. 2.b (which uses 800 triangles).

This test problem is simple in structure: three constant values separated by two shocks. We use it to test (i) the nonoscillatory property of our simplified local projection, (ii) the behavior of the numerical reflecting boundary condition at the lower boundary, and (iii) the effect when triangles are aligned with shocks.

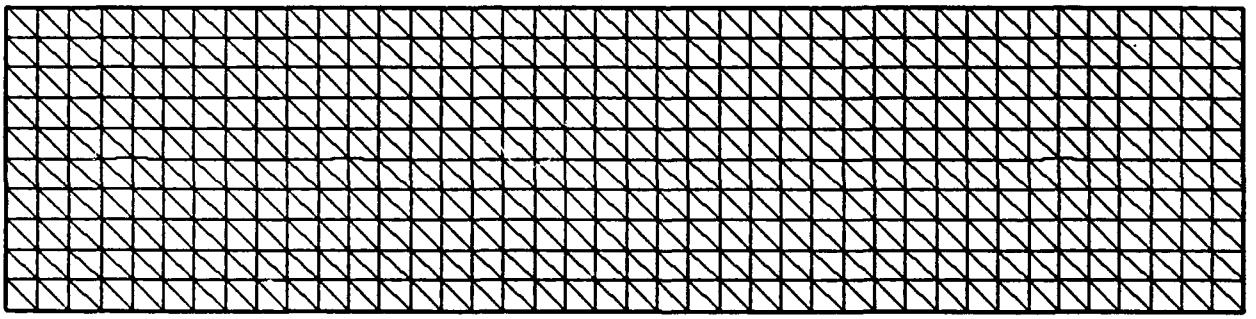

FIG. 2.A. *The triangulation '$\Delta x = \Delta y = 1/10$'. The pressure below has been computed on a triangulation four times finer than this one.*

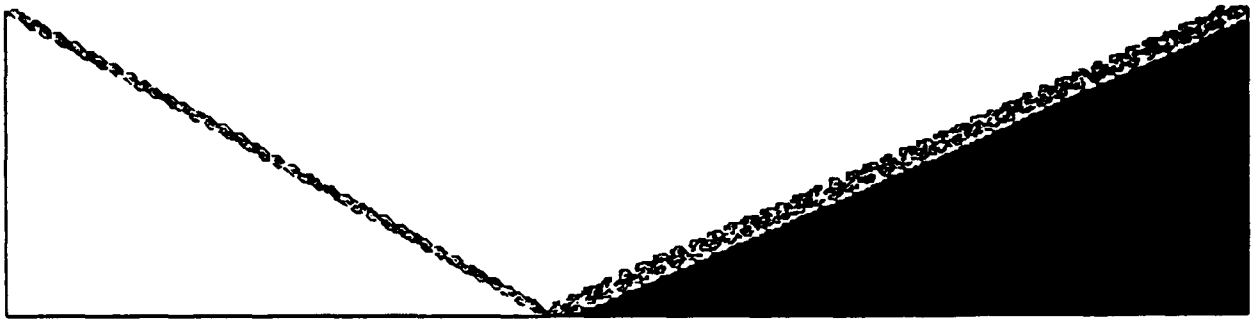

FIG. 2.B. *Pressure contour computed on the triangulation '$\Delta x = \Delta y = 1/40$'.*

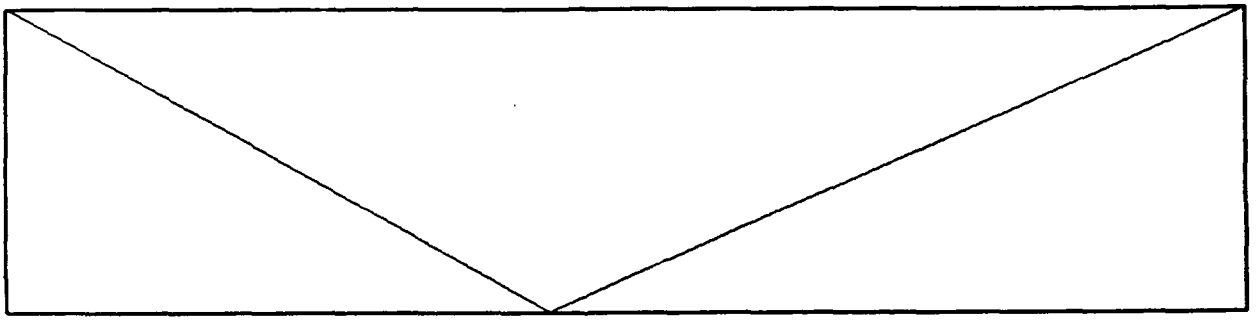

FIG. 2.C. *The triangles of this triangulation are aligned along the shocks of the exact solution.*

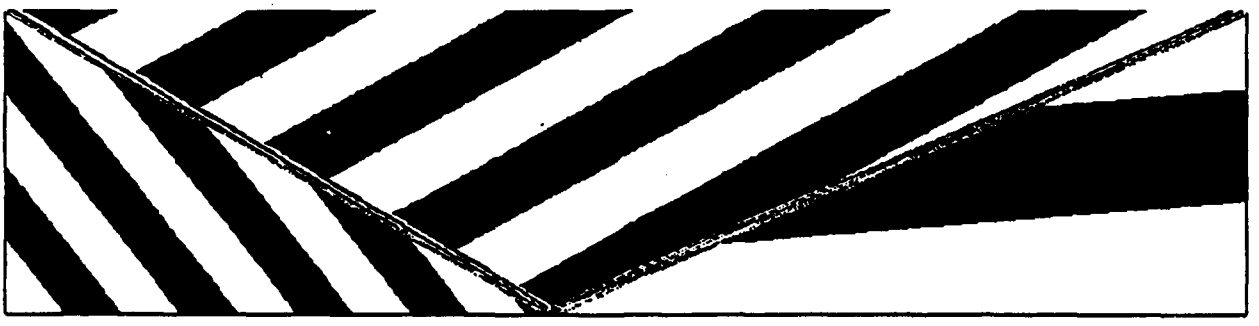

FIG. 2.D. *Pressure contours computed on the triangulation of Fig. 2.c.*

Example 2: Flow past a forward facing step. This is one of the two-dimensional problems Woodward and Colella [W] used to test the behavior of various finite difference schemes. The computational domain is $0 \leq y \leq 1$, $0 \leq x \leq \begin{cases} 0.6, & \text{if } y \leq .2 \\ 3.0, & \text{if} y > 0.2 \end{cases}$. The initial condition is a Mach 3 uniform flow: $\rho = 1.4, q_x = 3, q_y = 0, p = 1$ throughout the computational domain. The boundary conditions applied are: inflow at $x = 0$; outflow at $x = 3$; and reflecting at the walls $y = 1$, $y = 0$, $x = 0.6$ and $y = 0.2$. The corner is a singularity. In [W], Woodward and Colella suggested a way to numerically treat the singularity. We display results without, Fig. 3.b, and with, Fig. 3.c, such a treatment. Figs. 3.b and 3.c show the density contours at $T = 4$ computed with a refinement of the triangulation shown in Fig. 3.a corresponding to the Cartesian grid '$\Delta x = \Delta y = 1/40$'. We can see that our P^1–RKDG scheme produces results comparable with the same order MUSCL finite difference scheme using the grid '$\Delta x = \Delta y = 1/40$'.. We remark that since no sharpening technique is applied in the linearly degenerate field, the contact discontinuities are more seriously smeared than shocks. We are currently investigating the application of Yang's artificial compression ideas [Y].

Example 3: Double Mach reflection. This is the second example used in [W] to compare various finite difference schemes. We use a different computational domain (Fig. 4a) from the one used in [W]. Our domain is physically more natural and computationally easily manageable for triangulations. This is in contrast with finite difference methods which would meet complications in using our domain. The initial condition is described in Fig. 4a. It corresponds to a Mach 10 shock making 60 degrees with the bottom wall. The boundary conditions applied are: inflow at $x = 0$; outflow at $x = 3$; reflecting at the bottom; and the exact solution of a Mach 10 shock at the top. In Fig. 4c we show the density contour at $T = 0.2$. The triangulation used is drawn in Fig. 4b. Again , we do not try to align the triangles with the shocks, and the number of degrees of freedom used is close to the middle case ($\Delta x = \Delta y = 1/60$) in [W]. We again observe a result comparable with the finite difference schemes, except for the above mentioned smearing of contact discontinuities.

4. Concluding remarks. We have discussed the generalization of the RKDG method to two-dimensional systems of conservation laws, using the Euler equations of gas dynamics as an example. Numerical tests using P^1 elements on three standard examples show comparable results with nonoscillatory finite difference schemes and indicate good potential of our finite element method in handling geometry and boundary conditions.

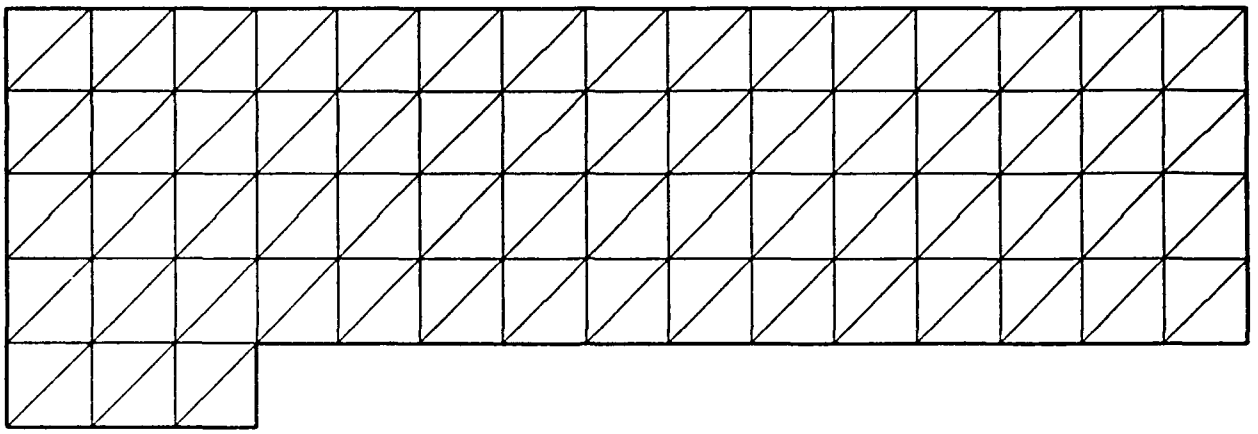

FIG. 3.A. *The triangulation '$\Delta x = \Delta y = 1/5$'. The densities below hve been computed on a triangulation eight times finer.*

FIG. 3.B. *Density contours computed on the triangulation '$\Delta x = \Delta y = 1/40$'. No treatment of the singularity at the corner is used.*

FIG. 3.C. *Density contours computed on the triangulation '$\Delta x = \Delta y = 1/40$'. The treatment of the singularity at the corner suggested in [W] is used.*

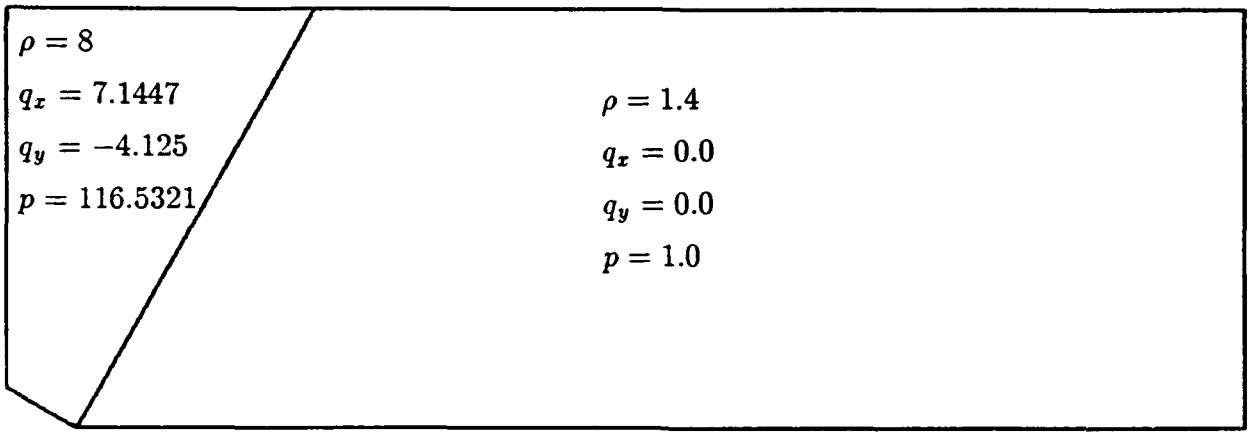

FIG. 4.A. *The computational domain and the initial conditions.*

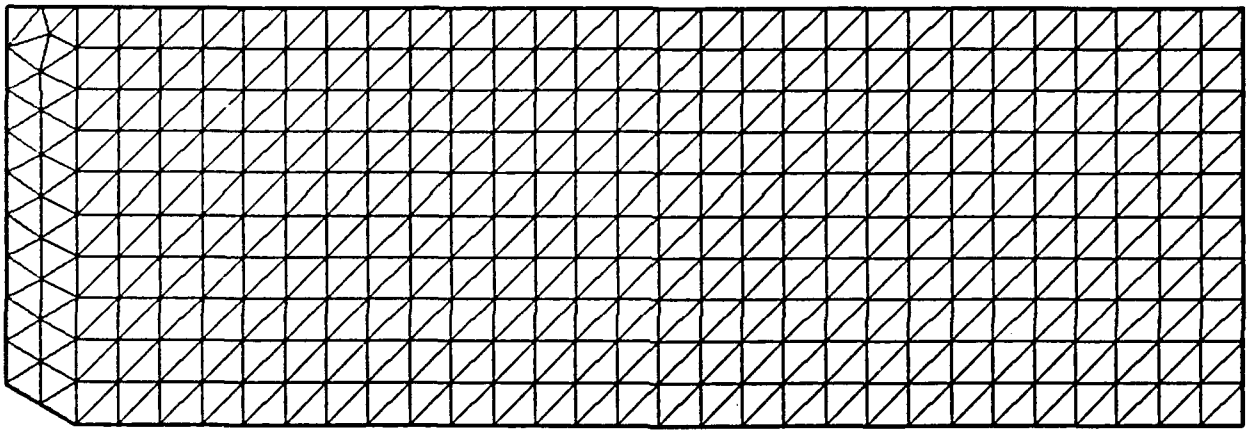

FIG. 4.B. *The triangulation '$\Delta x = \Delta y = 1/10$'. The density below has been computed of a triangulation six times finer.*

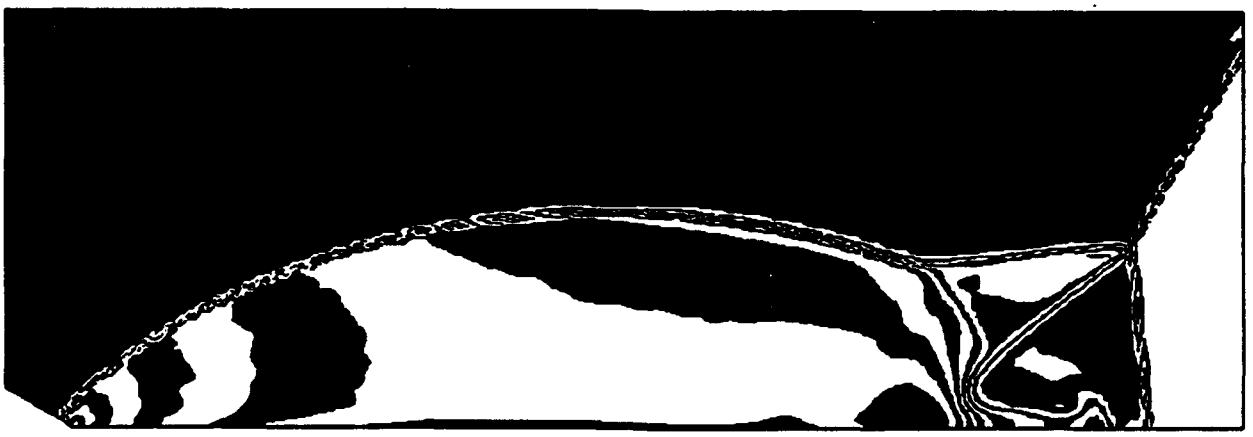

FIG. 4.C. *Density contours computed with the triangulation '$\Delta x = \Delta y = 1/60$'.*

REFERENCES.

[C1] B. COCKBURN AND C.W. SHU, *The Runge-Kutta Local Projection P^1-Discontinuous Galerkin Method for Scalar Conservation Laws*, M^2AN, 25 (1991).

[C2] B. COCKBURN AND C.-W. SHU, *TVB Runge–Kutta local projection discontinuous–Galerkin finite element method for conservation laws II: General framework*, Math. Comp., 52 (1989), pp. 411–435.

[C3] B. COCKBURN, S.Y. LIN AND C.W. SHU, *TVB Runge-Kutta Local Projection Discontinuous Galerkin Finite Element Method for Conservation Laws III: One Dimensional Systems*, J. Comput. Phys., 84 (1989), pp. 90–113.

[C4] B. COCKBURN, S. HOU, AND C.W. SHU, *TVB Runge-Kutta Local Projection Discontinuous Galerkin Finite Element Method for Conservation Laws IV: The Multidimensional Case*, Math. Comp., 54 (1990), pp. 545–581.

[Ro] P. ROE, *Approximate Riemann Solvers, Parameter Vectors, and Difference Schemes*, J. Comput. Phys., 43 (1981), pp. 357–372.

[S1] C.-W. SHU AND S. OSHER, *Efficient Implementation of Essentially Non-Oscillatory Shock-Capturing Schemes*, J. Comput. Phys., 77 (1988), pp. 439–471.

[S2] ———————, *Efficient Implementation of Essentially Non-Oscillatory Shock Capturing Schemes, II*, J. Comput. Phys., 83 (1989), pp. 32–78.

[W] P. WOODWARD AND P. COLELLA, *The numerical simulation of two-dimensional fluid flow with strong schocks*, J. Comput. Phys., 54 (1984), pp. 115–173.

[Y] H. YANG, *The artificial compression method*, J. Comput. Phys., 89 (1990), pp. 125–160.